(12)
B.S.

FLOW RESEARCH COMPANY

A DIVISION OF FLOW INDUSTRIES, INC.

HEADQUARTERS
P.O. Box 5040, 21414 - 68th Ave. S.
Kent, (Seattle), WA 98031 (206) 854-1370
Seattle Ex. 622-1500 TWX 910-447-2762

PRINCETON COMBUSTION LABS
P.O. Box 237
Plainsboro, NJ 08536
(609) 452-9200

EUROPE
53 Barton Rd., Blechley
Milton Keynes MK23B1 England
MK0908 71571/71572 Telex 826671

(12)

(14) FLOW-RR-80

FLOW RESEARCH REPORT NO. 80

(6) NUMERICAL SIMULATION OF BOUNDARY LAYER TRANSITION.

(9) Final rept. 1 Jul 75-30 Jun 76

BY

(10) STEVEN A. ORSZAG

(11) MAY 1977

(12) 35 p.

Flow Research Company
A Division of Flow Industries, Inc.
P.O. Box 5040
Kent, Washington 98031
(206) 854-1370

390 409

(15) *This work was supported by the Office of Naval Research under Contract No. N00014-76-C-0263, Task No. NR 061-233, ARPA Order No. 2924.

LB

Contract Number: N00014-76-C-0263

ARPA Order Number: 2924

Program Code Number: NR 061-233/7-31-75, 438

Name of Contractor: Flow Research Company, A Division of Flow Industries, Inc.

Effective Date of Contract: 1 July 1975

Contract Expiration Date: 30 June 1976

Amount of Contract: $84,364.00

Principal Investigator and Phone Number: Dr. Earll Murman, (206) 854-1370

Scientific Officer: Mr. Morton Cooper

Short Title of Work: Numerical Simulation of Boundary Layer Transition

Numerical Simulation of Boundary Layer Transition*

by

Steven A. Orszag

Consultant, Flow Research Company, Kent, Washington 98031

Abstract

The purpose of this research was to develop numerical simulations of boundary layer transition. One of the essential aspects of the work was to investigate carefully the appropriate boundary conditions and mathematical models that should be employed in the study of transition processes. The effects of three dimensionality, spanwise wavelength selection, and streamline curvature were also considered.

*This work was supported by the Office of Naval Research under Contract No. N00014-76-C-0263, Task No. NR 061-233, ARPA Order No. 2924.

1. Introduction

In this report, we summarize the results obtained under Office of Naval Research Contract No. N00014-76-C-0263, Task No. NR 061-233, ARPA Order No. 2924. The purpose of this research was to develop numerical simulations of boundary layer transition. One of the essential aspects of the work was to investigate carefully the appropriate boundary conditions and mathematical models that should be employed in the study of transition processes. The effects of three dimensionality, spanwise wavelength selection, and streamline curvature were also considered.

The direct solution of the Navier-Stokes equations for the study of transition involves much computation because three-dimensional effects are important (see section 3), and high resolution is required in the downstream and boundary layer directions. To economize in the solution of transition problems, we have developed a nonlinear stability theory that seems to account for the principal effects observed in our direct numerical simulations. This Galerkin approximation is discussed in section 4.

In this report we briefly summarize our results. Detailed expositions of our results are given in the publications cited in the references.

2. Boundary Conditions

The basic flow geometry of the numerical simulations of transition reported in section 3 is shown in figure 1. The flow enters the computational domain at $x = 0$ and exits at $x = L$ (normally $L = 50$ cm). The free stream is at $z = \infty$, while the rigid wall is at $z = 0$. In the spanwise-y direction, the unperturbed boundary layer flow is assumed uniform while the perturbed (transitional) flow is assumed to satisfy periodic boundary conditions. A typical calculation reported in section 3 involves the use of 257 grid planes to resolve the downstream x direction, 8 Fourier modes to resolve the spanwise-y direction, and 33 Chebyshev polynomials to resolve the boundary-layer z direction. We discuss the boundary conditions applied in each of the coordinate directions in more detail below.

Spanwise Direction - Periodicity

The assumption of periodicity in the spanwise direction is consistent with the Navier-Stokes equations in the sense that if the perturbed boundary layer flow is initially periodic in y at $t = 0$, then the flow stays periodic in y with the same period for all later times. This periodicity does not prevent the formation of localized vortex structures in the flow during the process of transition--localized vortex structures that do appear during time evolution must, however, appear periodically in the y direction. The assumption of spanwise periodicity does not seem to cause any serious difficulty or physical inconsistency in comparing our computations with laboratory experiments like those of Klebanoff, Tidstrom, and Sargent (1962).

Boundary Layer Direction - Mapping

We have discovered that an algebraic mapping of the semi-infinite domain above the flat plate located at $z = 0$ into the finite interval $(-1,1)$ gives remarkably efficient and accurate numerical computations. The algebraic mapping is

$$\hat{z} = \frac{z - H}{z + H} \quad , \tag{2.1}$$

where H is a scale parameter normally chosen to be twice the height at which the unperturbed velocity is one-half the free-stream value (for

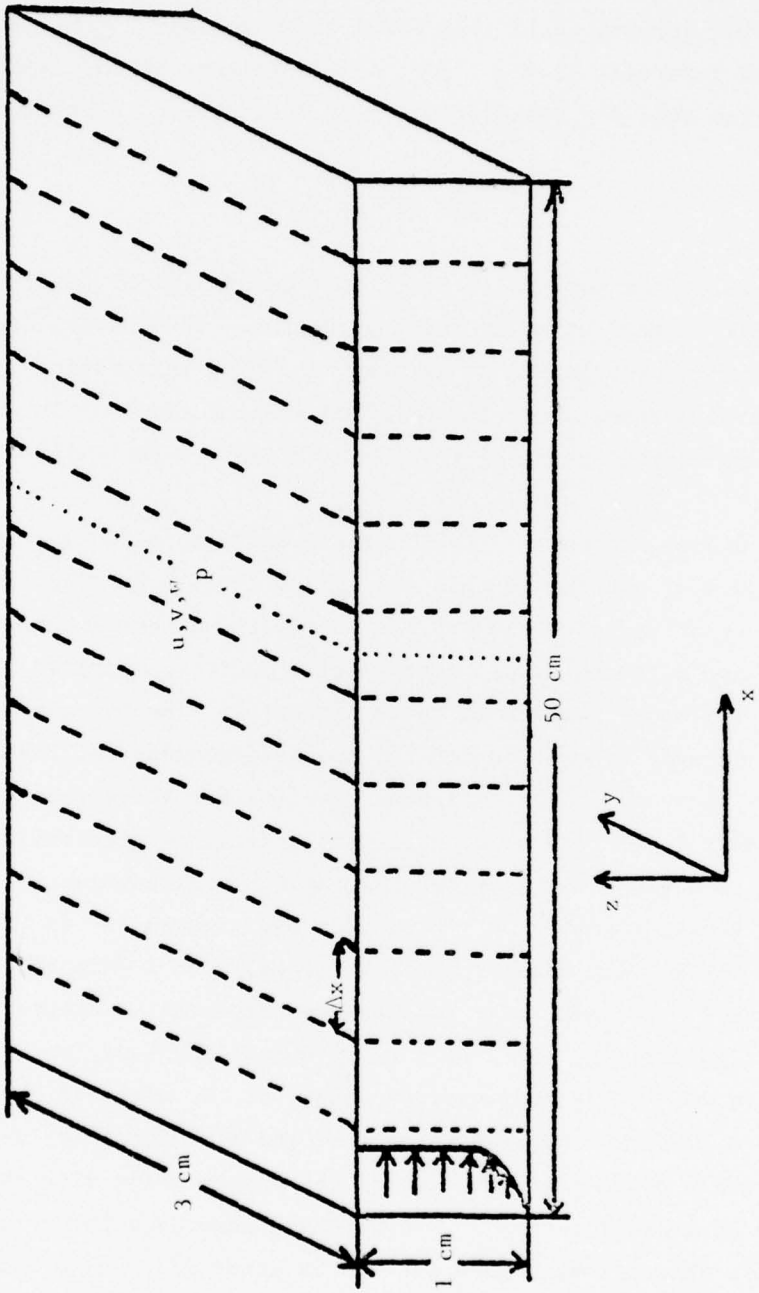

Figure 1 A plot of the computational domain for a typical run reported in section 3.

the Blasius boundary layer this height is approximated well by twice the displacement thickness of the boundary layer).

The mapping (2.1) transforms the interval $0 \leq z < \infty$ into the finite interval $-1 \leq z < 1$. A nice feature of the mapping (2.1) is that the rule for transformation of derivatives is simply

$$\frac{\partial u}{\partial z} = \frac{(1 - \hat{z})^2}{2H} \frac{\partial u}{\partial \hat{z}} \quad . \tag{2.2}$$

Basically, the mapping (2.1) is just an analytical device to introduce nonuniform resolution in the z direction. If a numerical scheme with uniform resolution in z is used, too much information is wasted in the free stream, where the solution changes slowly. This puts undue burdens on the numerical resolution closer to the wall, where the action lies.

Grosch and Orszag (1977) have given a detailed account of our analysis of mapping in this coordinate direction. They give a large variety of examples and explain in detail why the z direction is ripe for mapping techniques. Here we give just two examples that illustrate how well mapping works in the z direction. The two examples are the Orr-Sommerfeld equation for the linear eigenmodes of Blasius boundary layer flow and the Falkner-Skan equation for the stream function of boundary layer flow on wedges (with a pressure gradient).

In table I, we list the most unstable eigenvalue of Blasius flow at a Reynolds number $R = Ux/\nu = 580$, where x is the distance from the leading edge of the flat plate, with a (dimensionless) wave number of 0.179. Two numerical schemes are compared: a Chebyshev polynomial solution (Orszag, 1971) of the Orr-Sommerfeld equation truncated to the domain $0 \leq z \leq H$ for various values of H with the boundary condition $f' + 0.179f = 0$ applied to each of the eigenfunctions at $z = H$; and a Chebyshev polynomial solution of the same problem with the mapping (2.1) with scale factor $H = 1$. Note that, according to the discussion following (2.1), the optimal choice for H is about 3.4, so we could anticipate even greater accuracy by such a choice. (Here and in the rest of our work we non-dimensionalize z by the length scale $\sqrt{\nu x/U}$, where U

is the free-stream velocity, so the displacement thickness of the Blasius layer is 1.7.) Also note that it is not necessary to apply any boundary conditions at all at $\hat{z} = 1$ when using the mapping since eq. (2.2) ensures that all nonsingular derivatives vanish at $\hat{z} = 1$ after mapping.

Table I Eigenvalues of the Orr-Sommerfeld Equation For Blasius Flow

Mapping	H Scale Factor	N Number of Chebyshev Polynomials	C Eigenvalue
Restricted Domain	20	44	0.360213 + i0.006671
$0 \leq z \leq H$	30	44	0.364041 + i0.008113
Algebraic Mapping	1	26	0.364147 + i0.008007
$\hat{z} = (z-H)/(z+H)$	1	34	0.364121 + i0.007958
Exact Eigenvalue $c = 0.364123 + i0.007960$			

In Table II we list some errors in the value of $u(1)$, which is the non-dimensionalized x component of the velocity at a non-dimensionalized height of 1 above the rigid wall, as determined by numerical solution of the Falkner-Skan equation with only 11 grid points. Three different pressure gradients are listed in the table. For each case, the algebraic mapping achieves much better accuracy than that achieved by simply restricting the integration domain to $0 \leq z \leq H$. In table II, the points labelled * indicate that no acceptable (monotonic) solution to the discretized Falkner-Skan equation exists (with only 11 grid points).

Unfortunately, the technique of mapping works well only for problems where the solution is "simple" at infinity (see Grosch and Orszag (1977) for a variety of examples). Thus, boundary layer flows are "simple" at infinity because perturbations that are large near the wall die away exponentially fast as z increases. For example, if the amplitude of a linear mode of the Orr-Sommerfeld equation oscillates as $e^{i\alpha x}$, then its amplitude decreases like $e^{-\alpha z}$ for large z. On the other hand, the downstream x direction is not one in which the flow becomes "simple";

rather, we expect that sufficiently far downstream the flow will become turbulent. Mapping the semi-infinite x domain into a finite interval without considering the outflow boundary conditions will not work.

Table II Errors in Solution of the Falkner-Skan Equation

Mapping	H	β	Error in f'(1)
Restricted Domain	1.0	0	0.54
	2.5	0	0.052
	5.0	0	0.00013
	7.5	0	*
Algebraic Mapping	1.0	0	0.0000058
	2.5	0	-0.00000047
	5.0	0	-0.0000028
	7.5	0	-0.0000040
Restricted Domain	5.0	-0.1	0.00042
	7.5	-0.1	*
Algebraic Mapping	5.0	-0.1	-0.0000046
	7.5	-0.1	-0.0000064
Restricted Domain	2.5	0.1	0.032
	5.0	0.1	0.00014
	7.5	0.1	*
Algebraic Mapping	2.5	0.1	-0.0000055
	5.0	0.1	-0.000011
	7.5	0.1	-0.000016

[1] Solutions of the Falkner-Skan equation obtained by using 11 equally spaced grid points in the appropriate coordinate system. Here * indicates that no acceptable (monotonic) solution was found. Also, $f'(1) = u(1)/U$, the relative x velocity at a non-dimensional height of 1; $\pi\beta$ is the included angle of the analogous wedge flow.

Inflow-Outflow Boundary Conditions

Orszag (1974) has shown that the viscous Navier-Stokes equations are well posed if all three velocity components are specified at inflow and outflow boundaries. Orszag also showed that the inviscid Navier-Stokes equations are well posed if all three velocity components are specified at inflow points and if either the normal component of the velocity or the pressure is specified at an outflow point. We have investigated in

detail the effects of various boundary conditions on solutions of the Navier-Stokes equations and have developed new boundary conditions that minimize the effect of arbitrarily specified outflow boundary conditions on the flow in the interior of the domain of interest. A detailed report on our studies is being prepared (Orszag and Israeli, 1977); a preliminary outline of our results was published by Orszag (1976).

A simple model of viscous effects is given by the linearized Burgers' equation:

$$\frac{\partial u}{\partial t} + U \frac{\partial u}{\partial x} = \nu \frac{\partial^2 u}{\partial x^2} \quad , \tag{2.3}$$

where U is a constant advecting velocity and ν is the kinematic viscosity. Suppose we wish to solve eq. (2.3) on the semi-finite domain $0 \leq x < \infty$, and suppose that $U > 0$ so that $x = 0$ is an inflow point. Let us see what happens if the domain is truncated to the finite interval $0 \leq x \leq 1$. If ν is very small, the Laplace transform solution of the initial-value problem for eq. (2.3) is composed of modes of the form

$$u(x,t) = e^{\lambda x + \sigma t} \quad , \tag{2.4}$$

where the dispersion relation

$$\nu\lambda^2 - \lambda U - \sigma = 0 \tag{2.5}$$

determines λ as a function of σ. Thus, if $\nu << 1$, there are two possible modes given approximately by

$$\lambda_1 \sim U/\nu \tag{2.6}$$

$$\lambda_2 \sim - \sigma/U \quad . \tag{2.7}$$

The first mode λ_1 is a viscous mode that decays as $-x$ increases. The second mode λ_2 is a mode that describes propagation from $x = 0$ to $x = + \infty$.

The general solution to eq. (2.3) is of the form

$$u(x,t) = \int d\sigma e^{\sigma t} \left[A_1(\sigma) e^{\lambda_1 x} + A_2(\sigma) e^{\lambda_2 x} \right] . \tag{2.8}$$

When the semi-infinite domain $0 \leq x < \infty$ is truncated to the finite interval $0 \leq x \leq 1$, it is necessary to impose boundary conditions at both $x = 0$ and $x = 1$, say $u(0,t) = f(t)$ and $u(1,t) = 0$. Since λ_1 is large and positive, it follows from eq. (2.8) that the effect of this mode at $x = 0$ is exponentially smaller than its effect at $x = 1$. Therefore, neglecting the mode λ_1, we find from eq. (2.8) that the boundary condition $u(0,t) = f(t)$ determines $A_2(\sigma)$. On the other hand, the boundary condition $u(1,t) = 0$ determines $A_1(\sigma)$ in terms of $A_2(\sigma)$:

$$A_1 = -A_2 \exp(\lambda_2 - \lambda_1) . \tag{2.9}$$

Now we can compare the finite and semi-infinite problems. In the semi-infinite problem the mode λ_1 does not appear at all, but the solution is otherwise the same as for the finite problem. Therefore, according to eqs. (2.8) and (2.9) the effect of the boundary condition imposed at $x = 1$ is confined to a boundary layer of width of order ν/U near $x = 1$.

The boundary condition $u(1,t) = 0$ affects the solution only in the thin boundary layer with width of order ν/U. It is possible to decrease the effect of the artificial boundary at $x = 1$ still further by imposing a boundary condition of the form

$$\frac{\partial^k}{\partial x^k} u(1,t) = 0 \tag{2.10}$$

at $x = 1$. In this case, the solution for A_1 that corresponds to eq. (2.9) is

$$A_1 = -(\lambda_2/\lambda_1)^k A_2 \exp(\lambda_2 - \lambda_1) , \tag{2.11}$$

so the amplitude of mode 1 is a factor $(\nu/U)^k$ times smaller than with

straightforward application of $u(1,t) = 0$. The only danger in applying higher order conditions like eq. (2.10) with k large is that numerical instability may be induced by high order extrapolations near the outflow boundary. With numerically stable schemes, however, higher order boundary conditions should be more accurate than lower order boundary conditions.

We can make a similar analysis of a model problem that bears much closer relation to incompressible fluid mechanics than does eq. (2.3). The model includes the effect of pressure, which is essential for understanding the nature of the Navier-Stokes equations. The model consists of the two-dimensional linearized Navier-Stokes equations with a solution assumed to be of the special form

$$u = u(x,t)e^{iky} \quad , \quad v = v(x,t)e^{iky} \quad . \tag{2.12}$$

The model equations are given by

$$u_t + Uu_x + ikVu = - p_x + \nu(u_{xx} - k^2u) \quad , \tag{2.13}$$

$$v_t + Uv_x + ikVv = - ikp + \nu(v_{xx} - k^2v) \quad , \tag{2.14}$$

$$u_x + ikv = 0 \quad , \tag{2.15}$$

where we assume that $U > 0$ so $x = 0$ is an inflow boundary and V is arbitrary. We want to study the effect of truncating the semi-infinite domain $0 \leq x < \infty$ into the finite domain $0 \leq x \leq 1$. To do this, we analyze the Laplace transform solution of the initial value problem for eqs. (2.13)-(2.15).

The Laplace transform solution of eqs. (2.13)-(2.15) is composed of modes of the form

$$u(x,t) = ue^{\lambda x+\sigma t} \quad , \tag{2.16}$$

$$v(x,t) = ve^{\lambda x+\sigma t} \quad , \tag{2.17}$$

where the dispersion relation

$$(\lambda^2 - k^2)(\sigma + \lambda U + ikV - \nu\lambda^2 + \nu k^2) = 0 \qquad (2.18)$$

determines λ as a function of σ. The four roots of eq. (2.18) for given σ, k, U, and V are

$$\lambda_1 = +k, \quad \lambda_2 = -k \quad , \qquad (2.19)$$

and λ_3, λ_4 are the solutions of the quadratic equation

$$\nu\lambda^2 - \lambda U - (\sigma - ikV - \nu k^2) = 0 \quad .$$

When $\nu \ll 1$, the asymptotic behaviors of λ_3 and λ_4 are given by

$$\lambda_3 \sim U/\nu \ , \quad \lambda_4 \sim -\frac{\sigma + ikV}{U} \quad . \qquad (2.20)$$

The general solution of eqs. (2.13)-(2.15) is of the form

$$u(x,t) = \int d\sigma \, e^{\sigma t} \left[A_1(\sigma)e^{\lambda_1 x} + A_2(\sigma)e^{\lambda_2 x} + A_3(\sigma)e^{\lambda_3 x} + A_4(\sigma)e^{\lambda_4 x} \right] \quad . \qquad (2.21)$$

In the semi-infinite domain only modes 2 and 4 survive if the solution is bounded at ∞, so eq. (2.21) reduces to

$$u(x,t) = \int d\sigma \, e^{\sigma t} \left[A_2(\sigma)e^{\lambda_2 x} + A_4(\sigma)e^{\lambda_4 x} \right] \quad . \qquad (2.22)$$

In the finite domain $0 \leq x \leq 1$, all four modes are present to some extent and are determined by the boundary conditions. The contribution of mode 3 decays in a viscous boundary layer around the outflow boundary at $x = 1$ (as for the linearized Burgers' equation), so if ν is small, this mode causes negligible error throughout the interior of the interval $0 \leq x < 1$. On the other hand, the mode $\lambda_1 = +k$ is a pressure mode that decays appreciably only over the distance $1/k$, so if k is not large, its effect may be large over the whole computational domain. It is mode 1 that is the origin of the principal differences between the semi-infinite flow case and the finite-domain simulation.

There are several ways to minimize the effect of mode 1. One way is to assume that the computational domain has a large aspect ratio $L/H \gg 1$, where L is the length of the computational region and H is its height. In this case the smallest allowable transverse wavenumber k satisfies $k + 2\pi/H \gg 1/L$, so that mode 1 does in fact "boundary layer" (in a distance of order H) about the outflow boundary $x = L$. Thus, so long as $L - x \gg H$, the effect of arbitrarily specified outflow boundary conditions at $x = L$ is negligible.

Another way to limit the effect of the outflow boundary conditions is to modify the equations of motion in the neighborhood of the outflow boundary so that the "bad" mode 1 boundary layers in a thin boundary layer near $x = 1$. We therefore make the wavenumber of mode 1 become $\lambda_1 \gg 1$. Three ways to modify the Navier-Stokes equations to accomplish this wavenumber are:

(i) Replace the incompressibility condition $u_x + v_y = 0$ by $u_x + v_y = \mu \vec{v}\cdot\vec{n}$, where $\mu \gg 1$, and $\vec{n}$ is the outward normal.

(ii) Modify the pressure term in the Navier-Stokes equations to be $-\vec{\nabla}p + \mu\vec{n}p$.

(iii) Introduce pseudo-compressibility terms in the Navier-Stokes equations near the outflow boundary.

For example, if we replace eq. (2.15) by

$$u_x + ikv = \mu u \quad , \tag{2.23}$$

modes 3 and 4 of eqs. (2.13), (2.14), and (2.23) are unchanged from eq. (2.20), while modes 1 and 2 are replaced by

$$\lambda_1 \sim \mu \ , \quad \lambda_2 \sim -k^2/\mu \quad , \tag{2.24}$$

when $\mu \gg 1$. Thus, the size of λ_1 is increased, and mode 1 boundary layers near $x = 1$. To minimize the effect of the outflow boundary at $x = 1$, we choose $\mu(x)$ such that the effects of mode 1 are localized near $x = 1$.

This technique has been tested on the problem of low Reynolds number flow past a cylinder with mixed success. At a Reynolds number of four, when a truncation of the computational domain to $1 \leq r \leq r_\infty$ is used, the results for the drag coefficient C_D are as follows. Using the Imai asymptotic behavior of the vorticity and stream function as boundary conditions at r_∞, we obtain $C_D = 4.435$ if $r_\infty = 21.5$, $C_D = 4.441$ if $r_\infty = 35.0$, and $C_D = 4.442$ if $r_\infty = 59.1$. Using free-stream boundary conditions instead, we obtain $C_D = 5.13$ if $r_\infty = 21.5$, $C_D = 4.66$ if $r_\infty = 59.1$, showing the very large errors that can result from use of free-stream boundary conditions. On the other hand, the use of a modified Navier-Stokes equation of the form (i) with derivative boundary conditons applied at r_∞ and a quartic power law for $\mu(r)$ beyond $0.8r_\infty$, we obtain $C_D = 4.465$ if $r_\infty = 21.5$. However, if we use non-differentiated boundary conditions on the outer radius r_∞, then the best choice of $\mu(r)$ gives $C_D = 4.73$ at $r_\infty = 21.5$. Thus, with differentiated boundary conditions, the new methods appear to give superb results, while with non-differentiated boundary conditions, the results are less spectacular. A full discussion of these results and methods is given by Orszag and Israeli (1977).

3. Numerical Simulations of Boundary Layer Transition

In this section we describe some numerical results for boundary layer transition. In our earlier work on transition (Orszag, 1974), we solved a set of "parabolized" Navier-Stokes equations in which the x derivatives of the viscous dissipation terms were dropped on the basis that they were expected to be roughly 100 times smaller than the z-derivative contribution to the viscous terms in linear Tollmien-Schlicting waves. The advantage of the parabolized Navier-Stokes equations is that they allow the use of inviscid boundary conditions at the outflow boundary and prevent the occurrence of thin boundary layers near the outflow boundary. In the present work, we have compared the results of the parabolized Navier-Stokes equations with numerical solutions of the full Navier-Stokes equations and have found good agreement outside a thin boundary layer near the outflow boundary. The results presented below were all obtained by solution of the full Navier-Stokes equations.

Numerical Methods

The Navier-Stokes equations were solved by using 257 staggered grid planes in x with a compact mesh fourth-order difference operator (Orszag and Israeli, 1974). Inflow boundary conditions at $x = 0$ were that all three velocity components be specified (see below) and that outflow boundary conditions of various kinds be employed, including specification of $v = 0$, specification of $v_x = 0$, and specification of $v_{xx} = 0$. Most of the results reported below were obtained by using $v_x = 0$.

The y direction was resolved by using eight Fourier modes in a spectral representation (Gottlieb and Orszag, 1977). This representation ensures periodicity and gives an adequate representation of the initial stages of nonlinear growth before bursts actually appear. The bursts cannot be resolved by using only eight Fourier modes because they are very localized in y, so our calculations must be considered inadequate after the calculations predict bursts to occur. Nevertheless, our predictions of the location of transition should be good.

We resolve the boundary layer z direction by using an algebraic mapping together with a 33-mode Chebyshev polynominal expansion (Gottlieb and Orszag, 1977). Rigid boundary conditions are applied at $z = 0$, but no boundary conditions (other than boundedness) are applied at $z = \infty$. The advantages of Chebyshev polynominal solution of the z direction are that it is highly accurate, relatively easy to implement, and gives excellent resolution of any thin boundary layers that may appear.

Time stepping is done by a combination of methods. A semi-implicit algorithm is used in x to avoid stringent time-step restrictions imposed by outflow boundary layers (Gottlieb and Orszag, 1977, Haidvogel and Orszag, 1977). The semi-implicit scheme is combined with Adams-Bashforth explicit second-order time differencing on the advective terms and Crank-Nicolson implicit time differencing on the viscous terms. The overall time-stepping restrictions are not too severe and are of the form $\Delta t \lesssim \Delta x/u'$, where Δx is the spatial resolution in the interior of the computational domain and u' is the magnitude of a typical fluctuation velocity. In practice, accurate numerical results (as opposed to just stable ones) are obtained by taking the time step nearly 100 times smaller than this stability bound. To resolve accurately the advection effects of the unperturbed mean flow, we must take time steps that are comparable to the advection time of the mean velocity over one effective grid interval.

The pressure is solved by fast Fourier transform methods in x and y and a matrix inversion method in z. The matrix multiplication that is required is fast and accurate; the pressure computation requires about 25% of the overall time step.

The initial conditions we have used are those described by Orszag (1974). They consist of a superposition of a two-dimensional Tollmien-Schlicting wave and a three-dimensional Tollmien-Schlicting wave superposed on a Blasius profile, as suggested by the laboratory experiments of Klebanoff, Tidstrom and Sargent (1962) and the theory of Benney and Lin (Benney, 1964).

Transition on a Flat Plate

We have performed a series of numerical experiments on transition on a flat plate. The inlet of the computational domain is placed 1 m beyond the edge of a flat plate on which there is a zero-pressure gradient free-stream flow incident with $U = 1500$ cm/s . The kinematic viscosity is assumed to be 0.15 cm^2/s, the boundary layer thickness at the inlet is $\delta = \nu x/U = 0.099$ cm, the Reynolds number at the inlet is $R = U\delta/\nu = 1000$. The length of the computational domain is chosen to be 50 cm, and the scale height in the algebraic transformation (2.1) is chosen to be $H = 0.3$ cm .

The imposed primary Tollmien-Schlicting wave is chosen typically to be the unstable eigenmode of the Orr-Sommerfeld equation with wavelength 3.81 cm and has an imposed maximum u' fluctuation of $(0.01)U$. Various three-dimensional perturbations on this primary two-dimensional mode are investigated below; they typically consist of a $(0.0015)U$ ($(15\%)u'$) perturbation in the form of a three-dimensional Tollmien-Schlicting wave with the same x wavelength as the primary mode, but with various spanwise (y) wavelengths.

In a typical calculation, the time step is chosen to be $(0.002)s$, which is small compared with the primary Tollmien-Schlicting wave period of $(0.007)s$. The calculations proceed until a statistically steady state develops, normally after several hundred time steps.

In figure 2 we plot the results of a two-dimensional flow simulation with only the two-dimensional Tollmien-Schlicting wave applied. Observe that there is no explosive growth of the amplitude with increasing x , which indicates absence of transition.

In figure 3 we plot the results of a three-dimensional simulation in which the spanwise wavelength of the three-dimensional perturbation is 2.5 cm. In figure 4 we plot the results of a similar experiment in which the outflow boundary conditions $u_x = v_x = w_x = 0$ are replaced by $u_x = 0$, and $v = w = 0$.

In figures 5-7 we compare the mean velocity profiles at three locations in the flow whose perturbation amplitudes are plotted in figure 3. Observe that as the downstream distance increases, the flow

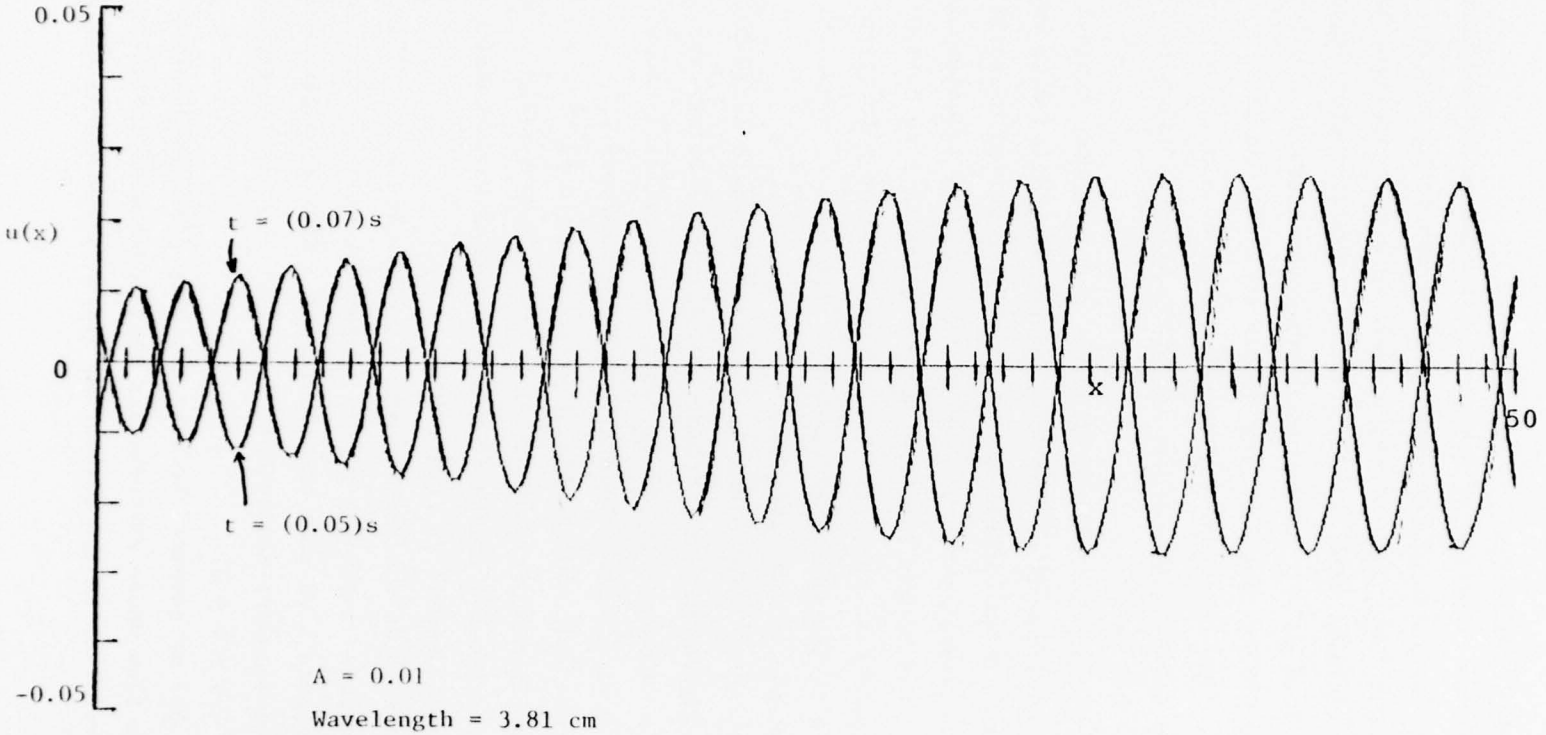

Figure 2 Growth of a Two-Dimensional Tollmien-Schlicting Wave

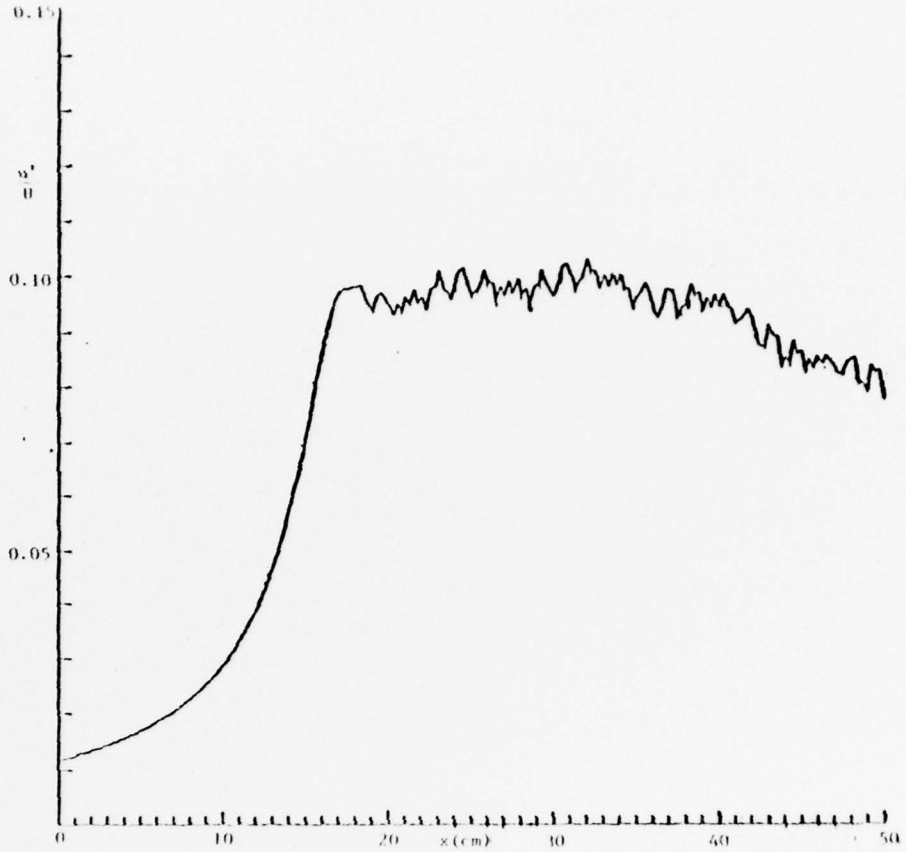

Figure 3 A plot of the relative disturbance amplitude u'/U , where U is the free-stream velocity, versus x for the boundary layer transition experiment described in the test. The plot is made at $t = (0.1)s$ for a flow in which $U = 1500$ cm/s , $\nu = 0.15$ cm^2/s , and the computational box begins at a distance $x_o = 1$ m from the leading edge of the flat plate. The cross-stream wavelength of the oblique disturbance is 2.5 cm at $x = 0$. Observe the abrupt transition $x \approx 20$ cm . The boundary conditions at outflow are $u_x = v_x = w_x = 0$.

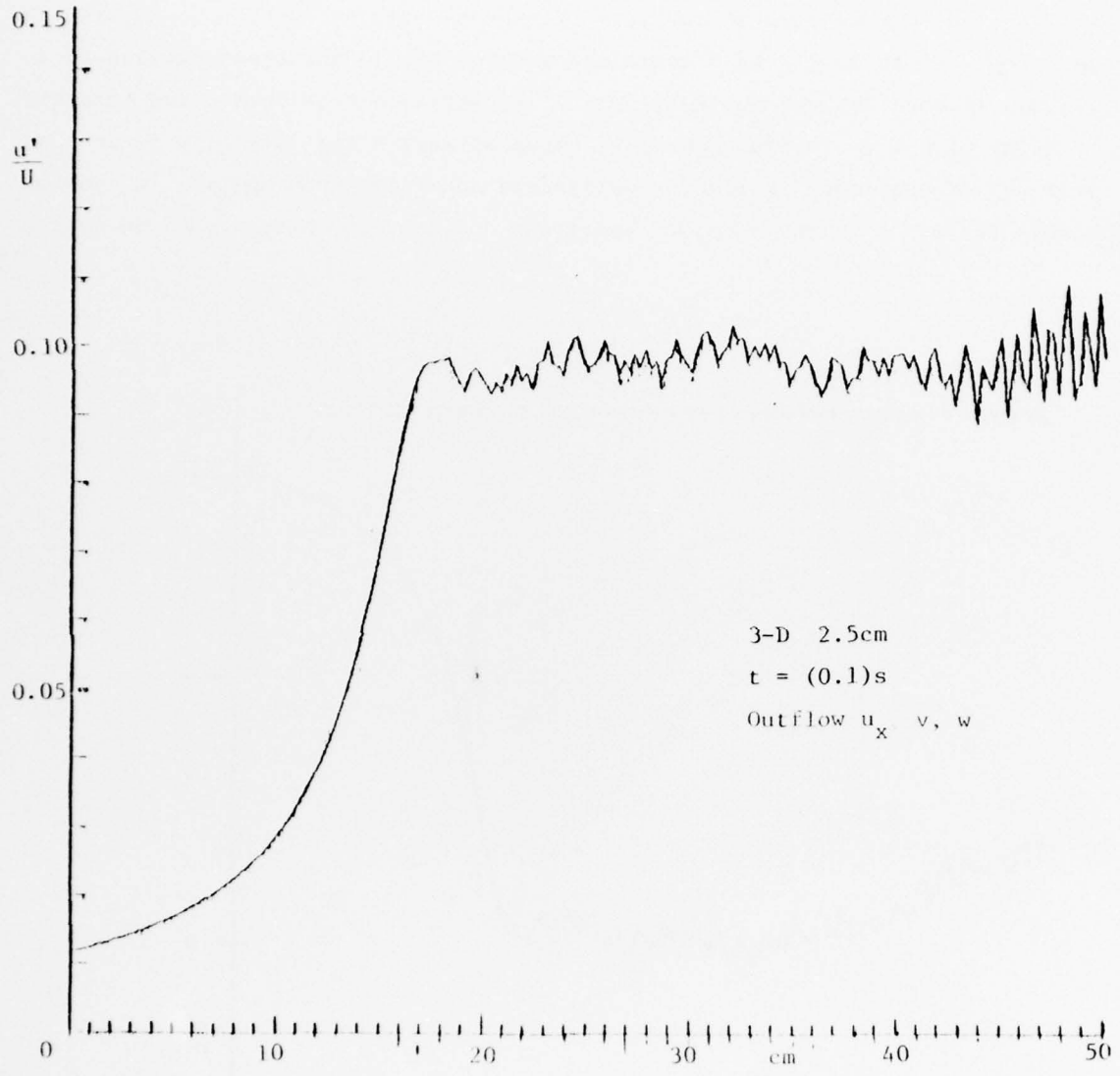

Figure 4 Growth of Maximum Amplitude of Perturbations in a Three-Dimensional Simulation With Modified Outflow Boundary Conditions

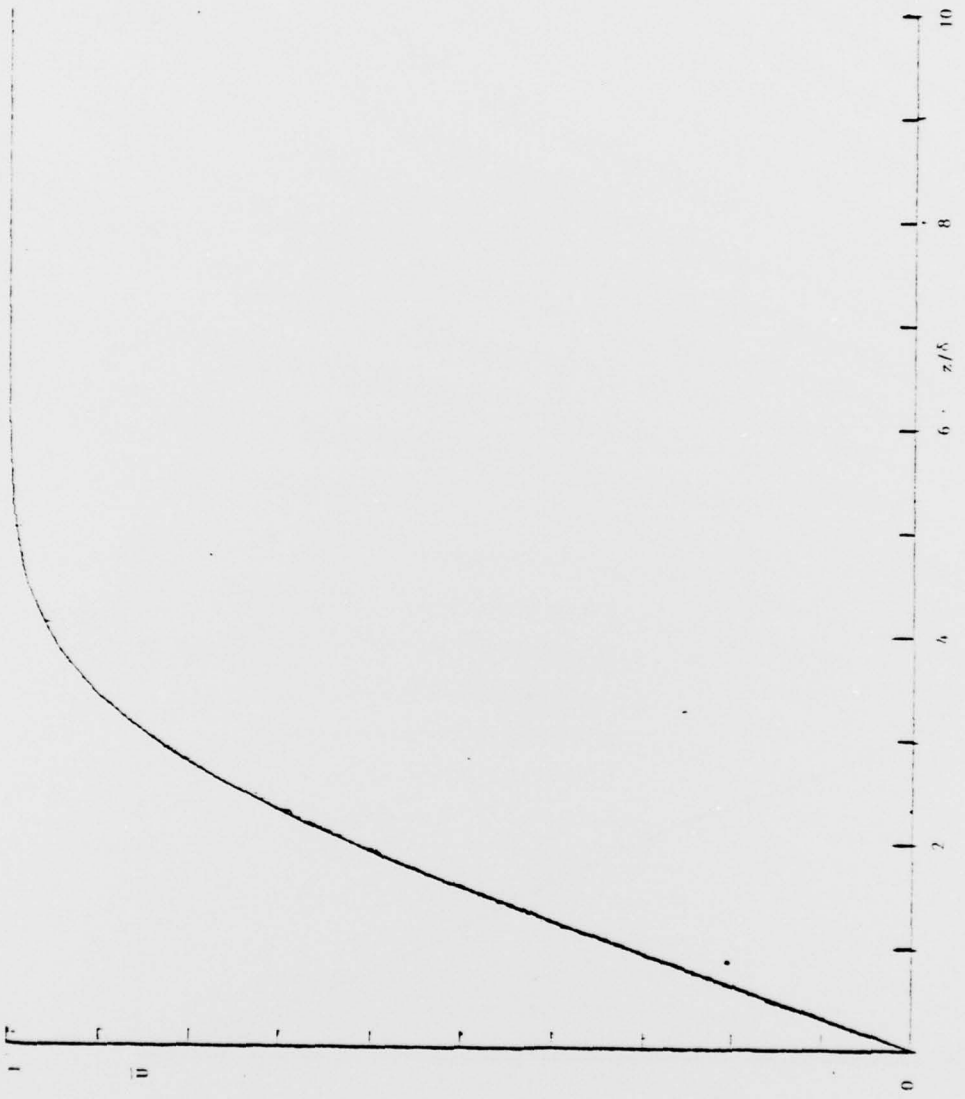

Figure 5 A plot of the mean velocity profile at x = 0 .

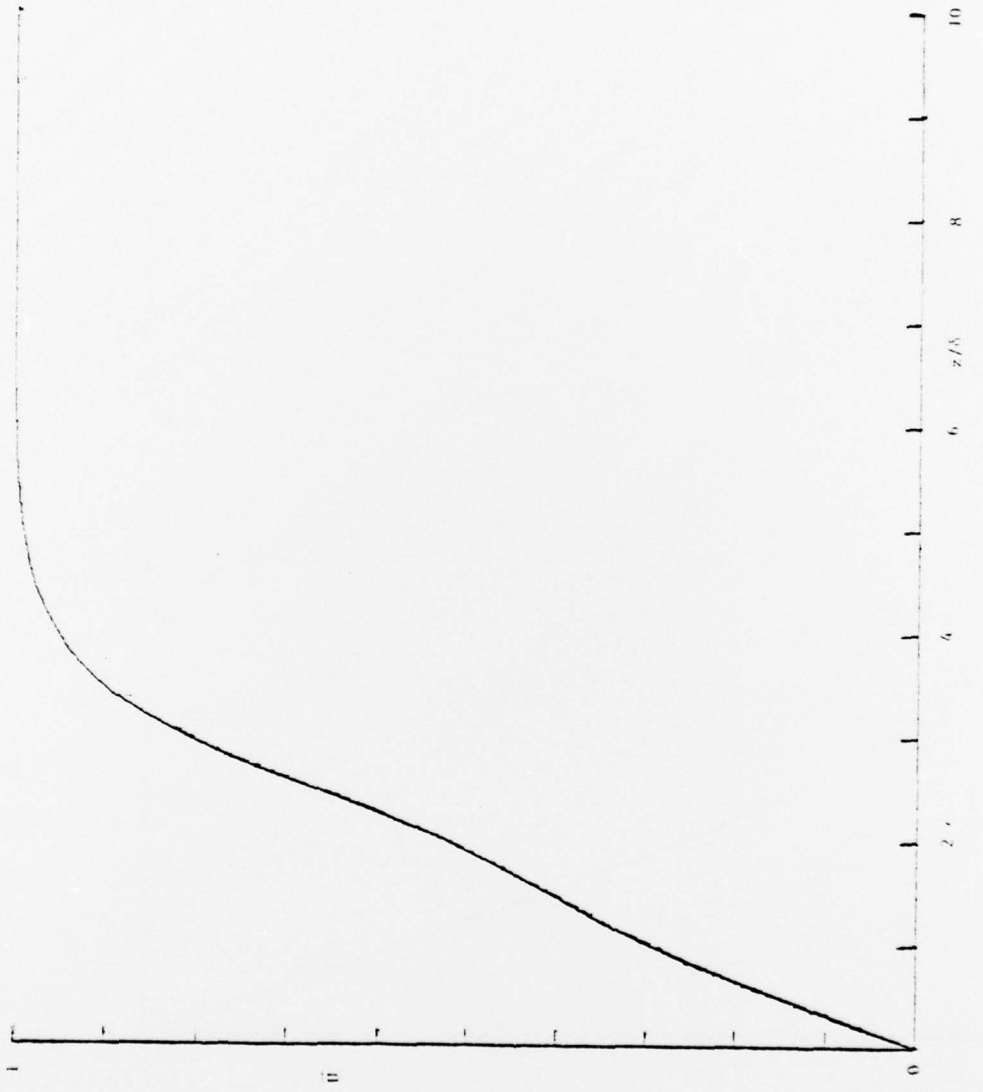

Figure 6 A plot of the mean velocity profile at x = 12.5 cm for the run plotted in figure 3.

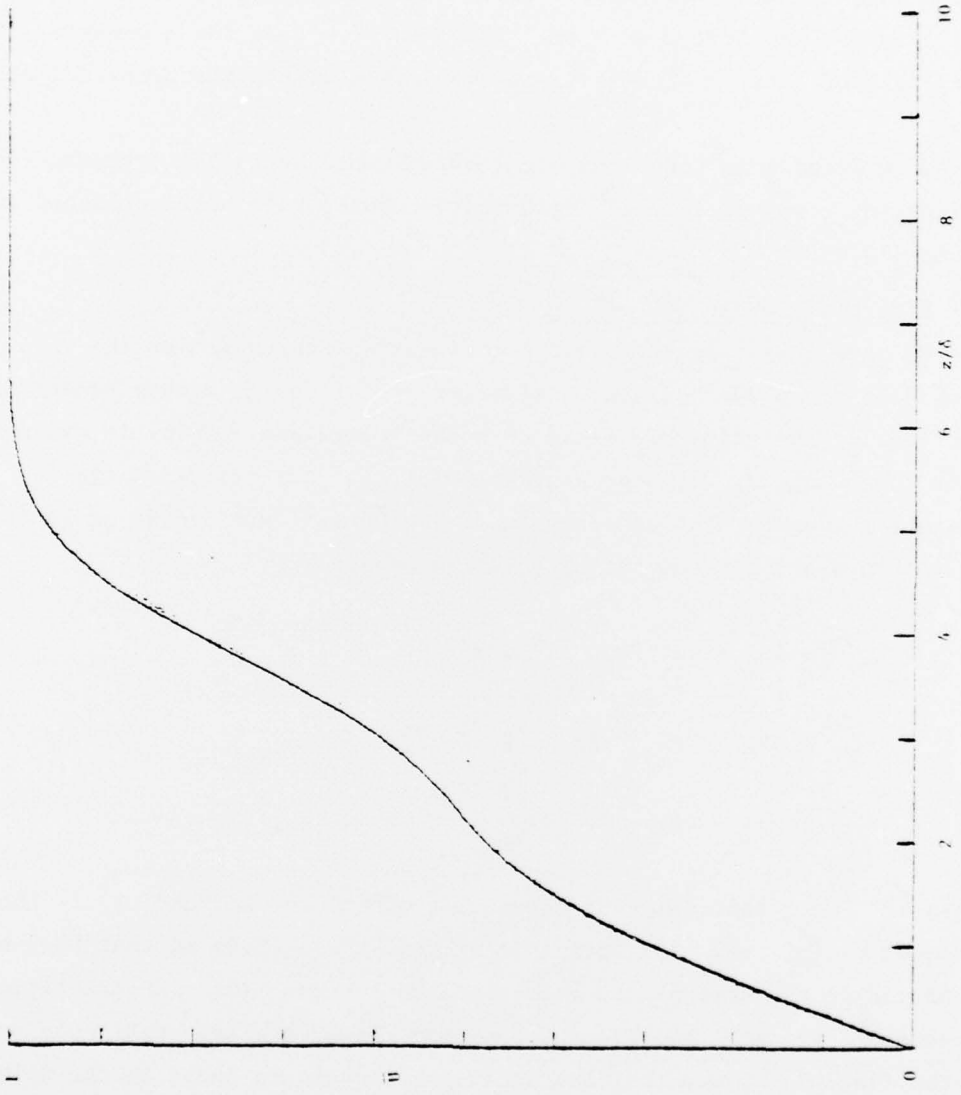

Figure 7 Same as figure 6, except plotted at x = 17.58 cm .

becomes highly inflectional at the spanwise location of the maximum velocity fluctuation. Beyond the point at which these highly inflectional profiles appear, we expect the rapid occurrence of bursts.

In figure 8 we show the effect of varying the spanwise wavelength on the location of transition. Observe the relatively broad minimum at a spanwise wavelength of 2 cm. Also, observe that for a spanwise wavelength of 7 cm, no transition was observed within the computational box.

More details on these numerical experiments are being prepared for publication (Orszag, 1977). Preliminary results have been published in Orszag (1976).

Effect of Surface Curvature

We have investigated the effect of surface curvature on the transition process by solving a modified set of Navier-Stokes equations that include the primary effects of such a curvature. Thus, in cylindrical coordinates, with the approximation that the radius r is constant throughout the boundary layer (which is justified if $r \gg \delta$, the thickness of the boundary layer), we obtain

$$\frac{\partial u}{\partial t} + uu_x + vu_y + wu_z + uw/R = -p_x + \nu\nabla^2 u \quad , \tag{3.1}$$

$$\frac{\partial v}{\partial t} + uv_x + vv_y + wv_z = -p_y + \nu\nabla^2 v \quad , \tag{3.2}$$

$$\frac{\partial w}{\partial t} + uw_x + vw_y + ww_z - \frac{u^2}{R} = -p_z + \nu\nabla^2 w \quad , \tag{3.3}$$

where ∇^2 also includes some terms that depend on R, and R is the constant radius r. The advantage of eqs. (3.1)-(3.4) is that they may be solved in the same planar geometry used for the flat plat transition experiments reported above. The boundary conditions are still $u = v = w = 0$ at the flat plate, and the same numerical techniques apply to the solution of the problem. The only difference is that the mean inflow generates longitudinal vorticity because of the curvature terms, and this longitudinal vorticity must be included in the numerical calculations. Thus, we ran the code for about 200 time steps to allow the longitudinal vorticity to develop, and then we applied the Tollmien-Schlicting waves (two- and three-dimensional) as perturbations.

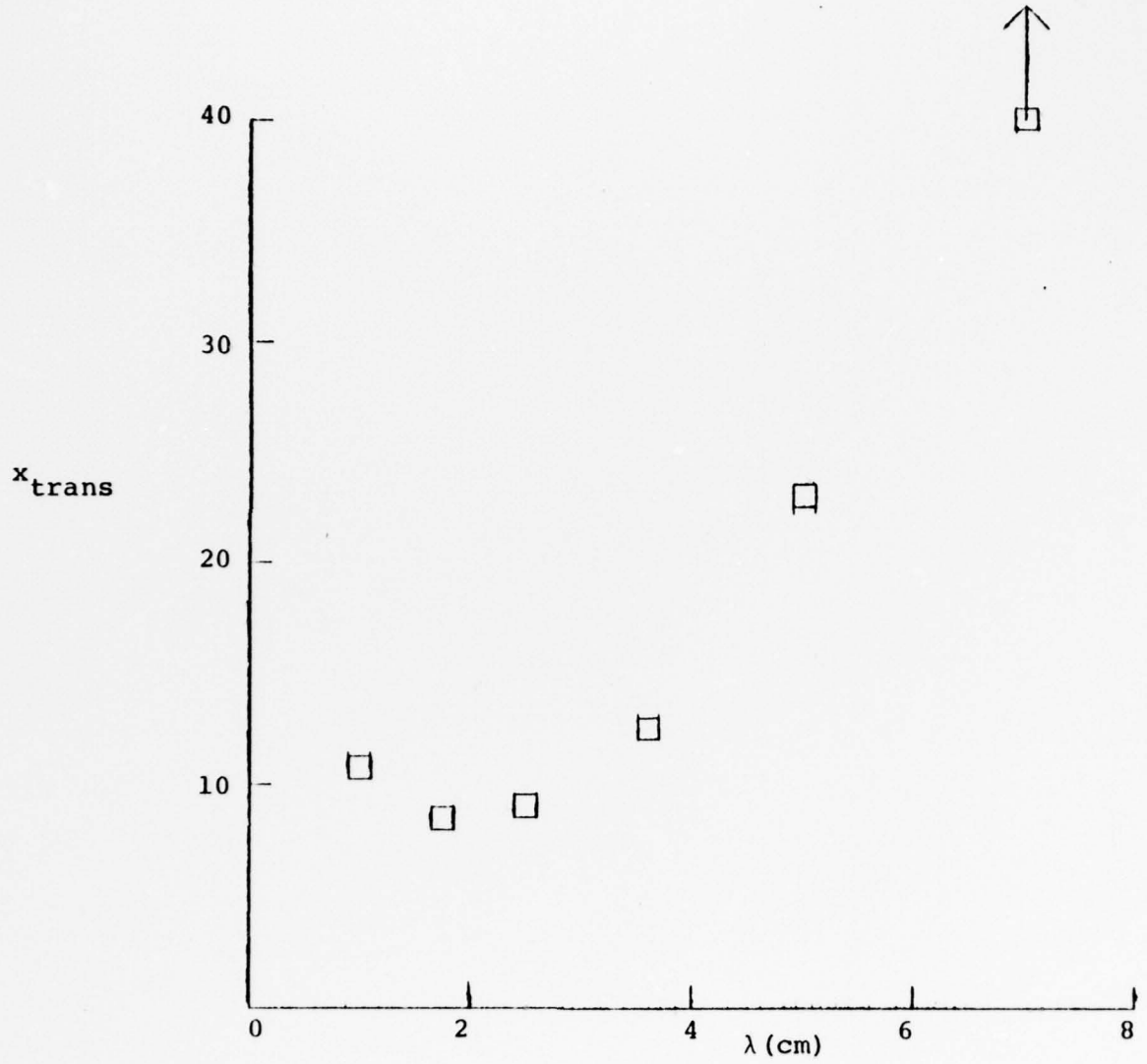

Figure 8 A plot of the location of the transition x_{trans} versus the cross-stream wavelength λ . The parameters of the boundary layer flow are as in figure 3. Observe that for $\lambda = 7$ cm , no transition was found within the computational box $0 \leq x \leq 50$ cm .

In figure 9 we show the results of a numerical experiment that is otherwise identical to the experiment plotted in figure 3, except that it includes the effects of concave surface curvature with $R = 15$ cm . Observe that the location of transition has been profoundly affected even though R is very large compared with the boundary layer thickness of 0.1 cm. Additional results of this kind are given by Orszag (1977).

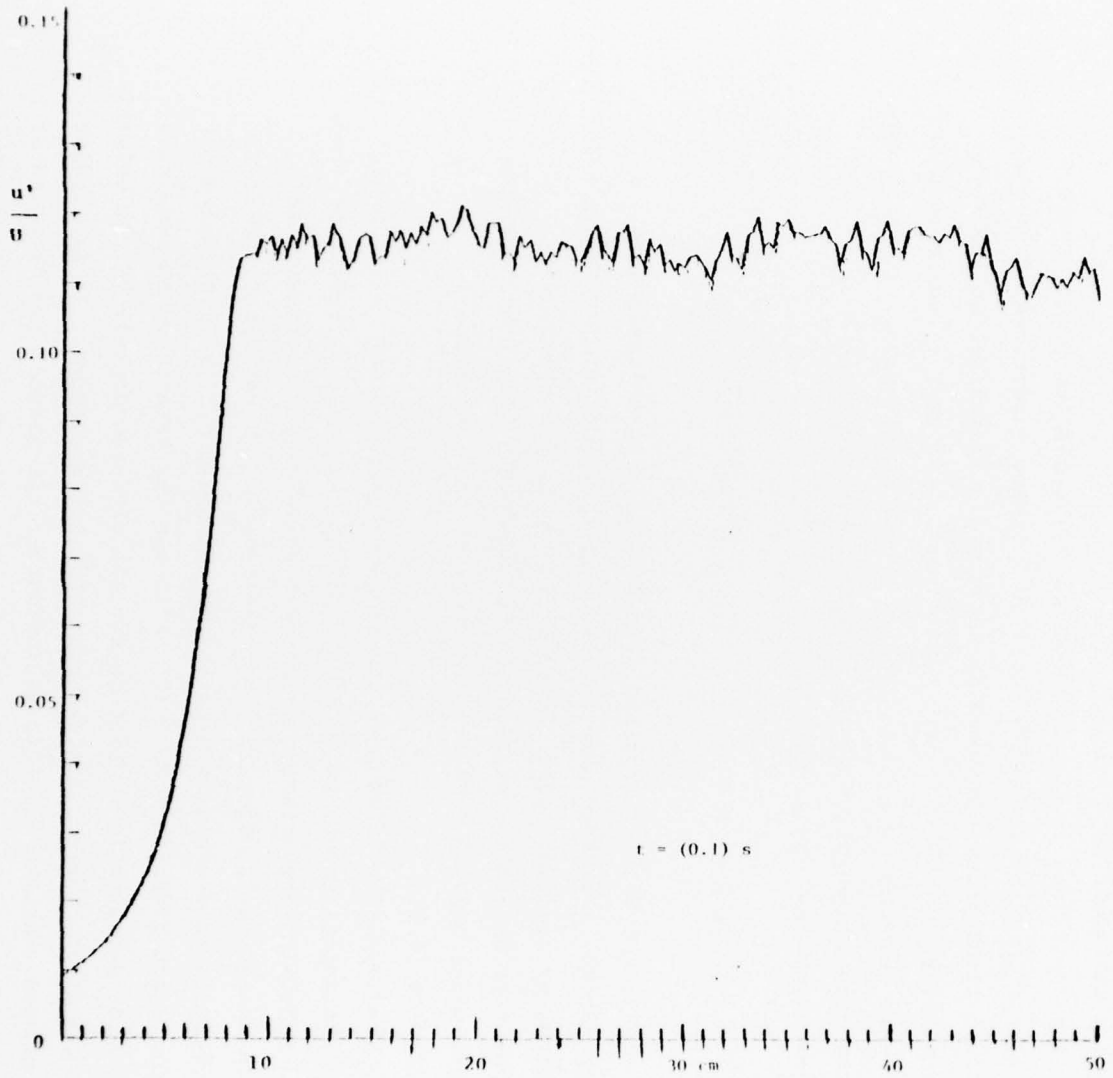

Figure 9 A plot of the amplitude of the maximum perturbation versus x in a calculation of transition on a concavely curved plate with radius of curvature R = 15 cm . The parameters of the calculation are otherwise the same as that case plotted in figure 3.

4. Galerkin Approximation

The idea of the Galerkin approximation method discussed here is similar to that of nonlinear stability theory. The nonlinear stability theory of boundary layer flows was worked out by Benney (1964) and subjected to numerical test by Antar and Collins (1975). Here we use a slightly different approach.

The basic idea is that the fundamental nonlinear dynamics are not grossly affected by the inflow-outflow boundary conditions imposed on the full simulations discussed in section 3. Therefore, we apply the much simpler periodic boundary conditions in x and y while retaining the rigid boundary conditions imposed in the z direction. In this case, we can seek the solution of the Navier-Stokes equations as a Fourier series in x and y as follows:

$$\vec{v}(x,y,z,t) = \sum_{|k|\leq K} \sum_{|p|\leq P} \vec{u}(k,p,z,t) e^{ikx+ipy} . \tag{4.1}$$

Next, the Fourier representation (4.1) is substituted into the Navier-Stokes equations, and equations for the Fourier components are obtained by equating coefficients of the various Fourier modes. Finally, a low-order Galerkin approximation is obtained by retaining only the lowest order modes and their harmonics, so the truncation $K = P = 2$ is applied to (4.1).

The resulting Galerkin approximation equations are solved numerically as differential equations in time, and the results are transformed back to a spatial representation by using a phase velocity transformation (even though the group velocity transformation is more justifiable). The results of a comparision with the three-dimensional simulation of figure 3 are given in figure 10. Although the details of the explosive growth of perturbation amplitude are not given accurately by the Galerkin approximation, the qualitative agreement is impressive. In particular, it appears that the Galerkin approximation can predict the location of transition to within approximately 20% even though the Galerkin approximation requires about two orders of magnitude less computer time than the direct solution of the Navier-Stokes equations.

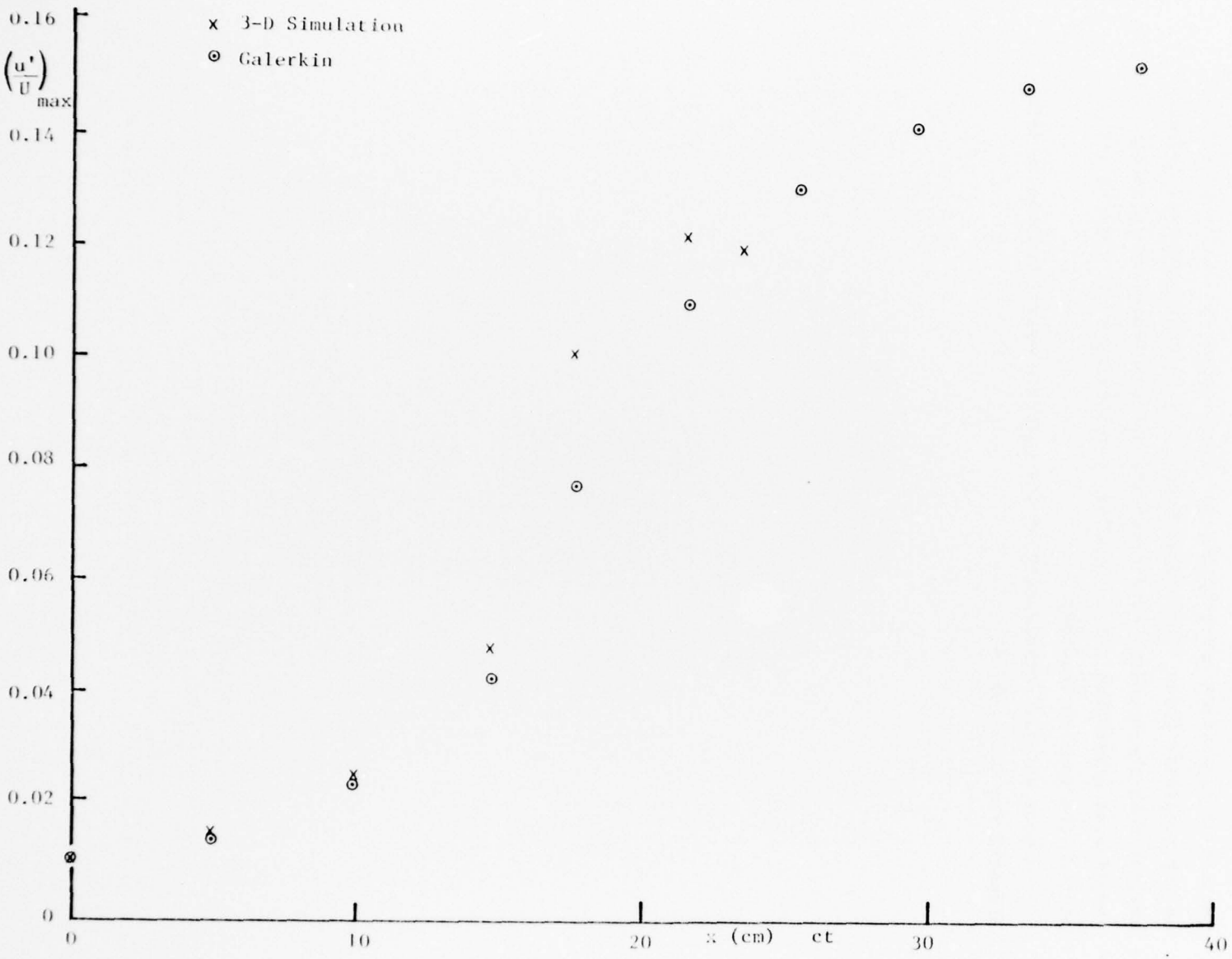

Figure 10 A comparison of the predictions of a Galerkin calculation with K = P = 2 and the full numerical simulation for the case plotted in figure 3.

The apparent success of the Galerkin approximation employed here is a very hopeful development. In particular, the full numerical simulations of transition are probably too complicated and costly to perform on any realistic three-dimensional body. The Galerkin results, however, suggest that the boundary conditions are not too important in detail, so complicated geometries can be studied by isolating small regions and piecing the results together.

A more detailed development of the Galerkin approximations is being prepared for publication.

References

Antar, B. N. and Collins, F. G. (1975) Phys. Fluids 18, 289.

Benney, D. J. (1964) Phys. Fluids 7, 319.

Gottlieb, D. and Orszag, S. A. (1977) "Numerical Analysis of Spectral Methods" SIAM/CBMS.

Grosch, C. E. and Orszag, S. A. (1977) to appear in J. Comp. Phys.

Haidvogel, D. and Orszag, S. A. (1977) to be published.

Klebanoff, P. S., Tidstrom, K. D. and Sargent, L. M. (1962) J. Fluid Mech. 12, 1.

Orszag, S. A. (1971) J. Fluid Mech. 50, 689.

Orszag, S. A. (1974) Flow Research Report No. 33.

Orszag, S. A. (1976) Proc. Fifth Intl. Conf. on Num. Methods in Fluid Dynamics, p. 32, Springer-Verlag.

Orszag, S. A. (1977) to be published.

Orszag, S. A. and Israeli, M. (1974) Ann. Rev. Fluid Mech. 6, 281.

Orszag, S. A. and Israeli, M. (1977) to be published.

SECURITY CLASSIFICATION OF THIS PAGE (When Data Entered)

REPORT DOCUMENTATION PAGE		READ INSTRUCTIONS BEFORE COMPLETING FORM
1. REPORT NUMBER Flow Research Report No. 80	2. GOVT ACCESSION NO.	3. RECIPIENT'S CATALOG NUMBER
4. TITLE (and Subtitle) Numerical Simulation of Boundary Layer Transition		5. TYPE OF REPORT & PERIOD COVERED Final 1 July 1975 - 30 June 1976
		6. PERFORMING ORG. REPORT NUMBER
7. AUTHOR(s) Steven A. Orszag		8. CONTRACT OR GRANT NUMBER(s) N00014-76-C-0263
9. PERFORMING ORGANIZATION NAME AND ADDRESS Flow Research Company, A Division of Flow Industries, Inc. P.O. Box 5040, Kent, WA 98031		10. PROGRAM ELEMENT, PROJECT, TASK AREA & WORK UNIT NUMBERS NR 061-233/7-31-75
11. CONTROLLING OFFICE NAME AND ADDRESS Office of Naval Research 800 North Quincy Arlington, Virginia 22217		12. REPORT DATE May 1977 13. NUMBER OF PAGES 31
14. MONITORING AGENCY NAME & ADDRESS(if different from Controlling Office) Defense Contract Administration Services District - Seattle Bldg. 5D, Naval Support Activity Sand Point, Seattle, WA 98115		15. SECURITY CLASS. (of this report) Unclassified 15a. DECLASSIFICATION/DOWNGRADING SCHEDULE

16. DISTRIBUTION STATEMENT (of this Report)

Distributed according to letter ONR:438:MC:mat, NR 061-223, 15 July 1977

DISTRIBUTION STATEMENT A
Approved for public release;
Distribution Unlimited

17. DISTRIBUTION STATEMENT (of the abstract entered in Block 20, if different from Report)

18. SUPPLEMENTARY NOTES

19. KEY WORDS (Continue on reverse side if necessary and identify by block number)

numerical simulation
boundary layer transition

20. ABSTRACT (Continue on reverse side if necessary and identify by block number)

The purpose of this research was to develop numerical simulations of boundary layer transition. One of the essential aspects of the work was to investigate carefully the appropriate boundary conditions and mathematical models that should be employed in the study of transition processes. The effects of three dimensionality, spanwise wavelength selection, and streamline curvature were also considered.

DD FORM 1 JAN 73 1473 EDITION OF 1 NOV 65 IS OBSOLETE

SECURITY CLASSIFICATION OF THIS PAGE (When Data Entered)